Clinical Imaging 53 (2019) 210–220

Contents lists available at ScienceDirect

Clinical Imaging

journal homepage: www.elsevier.com/locate/clinimag

Pediatric Radiology

Multi-phase 3D arterial spin labeling brain MRI in assessing cerebral blood perfusion and arterial transit times in children at 3T

Houchun H. Hu[a,*], Jerome A. Rusin[a], Ruiyue Peng[b], Xingfeng Shao[c], Mark Smith[a], Ramkumar Krishnamurthy[a], Bhavani Selvaraj[a], Danny J.J. Wang[c]

[a] Department of Radiology, Nationwide Children's Hospital, Columbus, OH, USA
[b] Translational MRI, LLC, Los Angeles, CA, USA
[c] Laboratory of FMRI Technology (LOFT), Stevens Neuroimaging and Informatics Institute, University of Southern California, Los Angeles, CA, USA

ARTICLE INFO

Keywords:
Pediatrics
Arterial spin labeling (ASL)
Arterial transit time
Cerebral blood flow (CBF)
Perfusion
Multi-delay/phase ASL

ABSTRACT

Background: 3D pseudocontinuous arterial spin labeling (pCASL) with a single post-labeling delay time is commonly used to measure cerebral blood flow (CBF). Multi-phase pCASL has been developed to simultaneously estimate CBF and arterial transit time (ATT).

Purpose: To evaluate the clinical feasibility of multi-phase 3D pCASL in pediatric patients, and to compare the estimation of ATT and CBF via linear weighted-delay and traditional non-linear iterative curve-fitting routines.

Material & methods: Forty patients (average age: 8.6 y, 5 d–22.4 y) referred for routine brain MRI underwent additional 5–7 min of pCASL scans at 3T using 5 PLDs between 300 and 2300 ms. Data were post-processed by two algorithms for estimating CBF and ATT. Average CBF and ATT values were computed for vascular territories including the anterior, middle and posterior cerebral arteries as well as regions based on the Alberta Stroke Program Early CT Score template. Pearson correlation coefficients and linear regression were used for statistical analysis. The clinical value of multi-phase CASL was evaluated by a neuroradiologist based on asymmetric CBF and ATT maps in patients.

Results: All pCASL scans were successfully completed, generating diagnostic results. CBF computed from weighted-delay and curve-fitting methods agreed strongly, with Pearson correlation coefficients ranging from 0.97–0.99 across the measured regions ($p < 0.05$). Correlation coefficients for ATT ranged from 0.87–0.96 ($p < 0.05$). CBF and ATT maps were found to add valuable information to clinical diagnosis in 17 of 40 pediatric patients.

Conclusion: Our preliminary results demonstrate the feasibility and potential clinical utility of multi-phase pCASL for simultaneous CBF and ATT quantification in pediatric patients.

1. Introduction

The use of arterial spin labeling (ASL) MRI to quantify tissue perfusion (in units of ml/100 g/min) has become increasingly popular over the past decade [1–9], as ASL facilitates non-invasive and repeatable examinations without the use of contrast agents. In a recent consensus paper endorsed by the International Society for Magnetic Resonance in Medicine and the European consortium for ASL in dementia, the use of a background suppressed 3D pulse sequence in conjunction with a pseudocontinuous ASL (pCASL) strategy has been recommended as the standard approach for clinical ASL applications [10]. ASL is particularly suitable for measuring cerebral blood flow (CBF) in children since no exogenous contrast agent is required and the signal-to-noise ratio of pediatric ASL is known to be higher in children than that in adults due to increased blood flow (except in newborns) and brain water. A growing number of studies have applied ASL to measure CBF in pediatric populations, including Moyamoya patients [11] and in patients with sickle cell anemia [12]. Additionally, ASL has been used to establish normative values during growth and development [13–15].

In the typical implementation of pCASL MRI, a single post-labeling-delay (PLD) is used. The PLD signifies the time between the labeling of blood by radiofrequency (RF) pulses, typically at the level of the carotid arteries, and the time when 3D data acquisition starts at the imaging volume. In the consensus paper by Alsop et al., a PLD of 2000 ms is

* Corresponding author at: Nationwide Children's Hospital, Department of Radiology, 700 Children's Drive, Columbus, OH 43205, USA.
E-mail address: houchun.hu@nationwidechildrens.org (H.H. Hu).

https://doi.org/10.1016/j.clinimag.2018.11.001
Received 2 September 2018; Received in revised form 10 October 2018; Accepted 2 November 2018
0899-7071/

Table 1
Summary of pertinent multi-delay pCASL pulse sequence parameters.

Parameter	Setting
Acquired orientation	Axial
Base sequence	3D GRASE
In-plane voxel size (mm)	2.5
Field-of-view (mm)	240
Matrix size	96–112
Number of slices in acquisition	30–40
Slice thickness (mm)	3–4
Slice oversampling	10%
Repetition time TR (msec)	4100
Echo time TE (msec)	36
Fat suppression	Frequency-selective
Partial echo/ partial Fourier	None
Bandwidth/pixel (Hz)	2480
EPI factor/turbo factor	63/4
Label bolus duration (ms)	1500
Label offset (mm)	75 for infants; 90 otherwise
Parallel imaging	None
Post labeling delays (PLD) (ms)	300, 800, 1300, 1800, 2300
Number of signal averages	3 per PLD
Number of label/control pairs	16
Scan time for given parameters (min)	5–7

recommended for neonates, 1500 ms for children, and 1800 ms for adults [10]. One limitation of the single-PLD pCASL exam is the potential appearance of low signal regions more distal to each perfusion territory. The low signal can be ambiguous, reflecting either low CBF or alternatively a prolonged arterial-transit-time (ATT) to that region from the RF labeling plane. Similarly, a single-PLD approach may be inadequate in capturing CBF in patients with asymmetric flow where one region or side of the brain has significantly different ATT than the rest or other side of the brain.

To overcome this limitation, multi-phase or multi-delay ASL methods have recently been introduced and are becoming increasingly used in clinical settings [16–20]. With data from multiple PLDs, the technique can provide simultaneously an ATT-corrected CBF map as well as a quantitative map of ATT. The product of CBF and ATT is arterial cerebral volume, or aCBV. Multi-phase ASL has been successful demonstrated in Moyamoya disease [21], and a recent study by Wang, et al. showed significant associations between ASL-derived CBF, arterial cerebral blood volume (CBV), ATT parameters and CT perfusion measurements of CBF, CBV, and mean transit time (MTT) [22]. Another study by Wang, et al. compared multi-delay ASL results with values derived from dynamic susceptibility contrast (DSC) MRI in acute ischemic stroke patients, showing statistically significant correlations between perfusion parameters by ASL and DSC [23]. Lou, et al. has

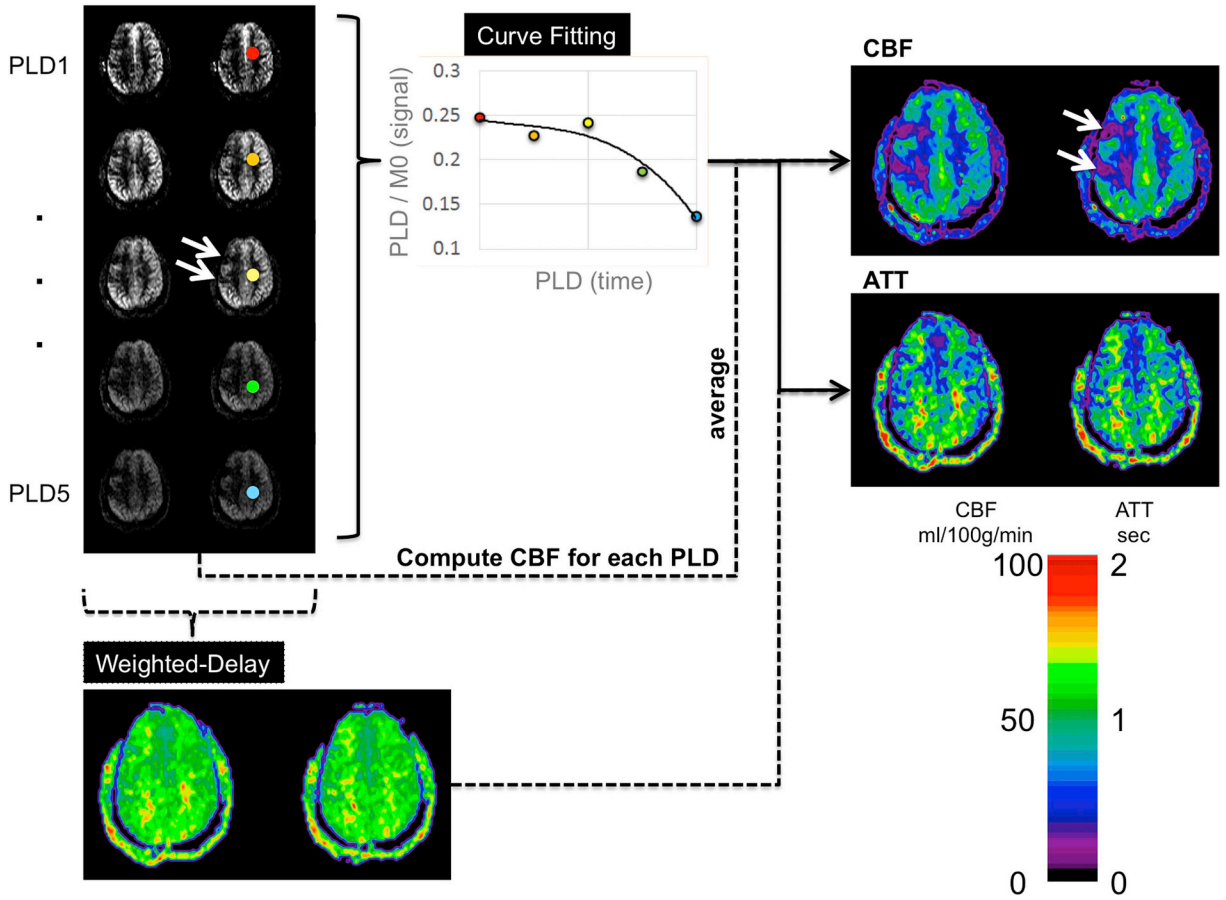

Fig. 1. Exemplary data from a 17 y female patient with a history of stroke. There are two perfusion deficits in the posterior right frontal lobe, which corresponds to foci of cystic encephalomalacia (arrows). Left top panel shows individual PLD data for two slices (from top to bottom: PLD = 500 ms + 500 ms increments). Remainder of figure shows the flow chart of how a weighted-delay routine (dashed arrow path) and an iterative curve fitting routine (solid arrow path) are used to generate CBF and ATT maps. CBF and ATT are shown using the same colorbar, but from 0 to 100 ml/100 g/min or 0–2 s, respectively. The weighted-delay is computed from the individual PLD data and is also in units of time (*sec*), shown on the same color scale as the ATT map. In the weighted-delay approach, individual CBFs are also computed for each PLD, and the final CBF is the group mean of the five estimated CBFs at each of the five PLDs (For interpretation of the references to color in this figure legend, the reader is referred to the web version of this article.).

Table 2
A summary of Pearson correlation coefficients (r^2) for regional CBF between linear weighted-delay mapping and non-linear iterative fitting computations. For each entry, slope (m) and intercept (b) are provided. Also provided in brackets are the 95% confidence intervals of the slope (m) and the intercept (b). Confidence intervals (CIs) that contain 1 for slope and 0 for intercept are italicized. All correlations were statistically significant with $p < 0.05$.

Perfusion territory	Left brain r^2/m/b [m: 95% CI], [b: 95% CI]	Right brain r^2/m/b [m: 95% CI], [b: 95% CI]
Anterior cerebral artery	0.99/0.94/1.49 [m: 0.90, 0.97], [b: 0.10, 2.85]	0.99/0.94/1.64 [m: 0.90, 0.97], [b: 0.36, 2.92]
Anterior choroidal artery	0.99/0.94/1.48 [m: 0.91, 0.98], [b: 0.39, 2.55]	0.99/0.94/1.72 [m: 0.91, 0.98], [b: 0.68, 2.77]
Posterior cerebral artery	0.98/0.96/1.51 [*m: 0.92, 1.0*], [*b: −0.01, 3.04*]	0.99/0.95/1.76 [m: 0.91, 0.98], [b: 0.42, 3.10]
Middle cerebral artery	0.99/0.91/2.27 [m: 0.87, 0.94], [b: 1.05, 3.48]	0.98/0.89/2.26 [m: 0.85, 0.94], [b: 0.74, 3.78]
Posterior communicating artery	0.98/0.95/1.10 [m: 0.91, 0.99], [*b: −0.18, 2.37*]	0.99/0.97/0.86 [*m: 0.93, 1.00*], [*b: −0.19, 2.0*]
Insula	0.98/0.91/2.12 [m: 0.87, 0.96], [b: 0.36, 3.88]	0.98/0.88/2.99 [m: 0.84, 0.93], [b: 0.95, 5.03]
Caudate nucleus	0.98/0.91/1.42 [m: 0.87, 0.96], [*b: −0.14, 2.99*]	0.97/0.90/2.11 [m: 0.85, 0.95], [b: 0.52, 3.70]
Lentiform nucleus	0.97/0.88/2.98 [m: 0.83, 0.92], [b: 1.18, 4.78]	0.98/0.89/2.84 [m: 0.85, 0.93], [b: 1.42, 4.27]
Internal capsule	0.97/0.86/2.81 [m: 0.80, 0.91], [b: 1.07, 4.55]	0.98/0.90/2.08 [m: 0.85, 0.94], [b: 0.57, 3.58]
M1	0.99/0.96/1.37 [*m: 0.92, 1.0*], [*b: −0.1, 2.83*]	0.98/0.95/1.75 [m: 0.90, 0.99], [b: 0.02, 3.47]
M2	0.99/0.92/2.16 [m: 0.89, 0.95], [b: 0.68, 3.63]	0.98/0.90/2.61 [m: 0.87, 0.94], [b: 0.85, 4.38]
M3	0.99/0.96/1.13 [*m: 0.92, 1.0*], [*b: −0.50, 2.76*]	0.99/0.94/1.87 [m: 0.90, 0.96], [b: 0.20, 3.54]
M4	0.98/0.98/1.15 [*m: 0.93, 1.03*], [*b: −0.68, 2.99*]	0.99/0.99/1.01 [*m: 0.94, 1.03*], [*b: −0.61, 2.63*]
M5	0.98/0.97/1.28 [*m: 0.92, 1.01*], [*b: −0.40, 2.97*]	0.98/0.96/1.25 [*m: 0.92, 1.00*], [*b: −0.36, 2.86*]
M6	0.99/1.01/0.20 [*m: 0.97, 1.04*], [*b: −1.25, 1.64*]	0.99/0.99/0.69 [*m: 0.95, 1.03*], [*b: −0.80, 2.18*]

applied multi-phase ASL to identify leptomeningeal collateral perfusion in stroke patients [24], while Chen G, et al. recently reported using this technique to study patterns of postictal cerebral perfusion in patients with idiopathic generalized epilepsy [25]. In a recent study by Choi, et al., the investigators demonstrated the clinical utility of multi-phase ASL in predicting cerebrovascular reserve [26], while MacIntosh, et al. has investigated the influence of remifentanil on CBF and ATT [27].

The primary purpose of this work was to demonstrate the feasibility of concurrent measurements of CBF and ATT in pediatric patients undergoing clinical 3T MRI exams at our tertiary pediatric referral hospital. A secondary purpose of this study was to compare two post-processing algorithms for estimating CBF and ATT using a linear weighted-delay approach and a nonlinear iterative least-squares curve-fitting approach from multi-delay 3D pCASL data. Such a comparison of CBF and ATT estimations has not been previously reported.

2. Material and methods

This HIPAA-compliant MRI study was approved by our institution's research and ethics board as a minimum-risk quality improvement project. Informed consent of parents and assent by child subjects (if applicable) were obtained to add the multi-phase 3D pCASL sequence to a standard-of-care morphological brain MRI exam, which included conventional T1, T2, fluid-attenuated T2, and diffusion weighted imaging. Data from 40 patients (18 boys, 24 girls, age range: 5 days–22.4 years, average age: 8.6 years) were included in this study from July 2017 to April 2018. All patients were referred for a standard brain MRI for clinically indicated reasons. Seventeen patients received general anesthesia following institutional protocol. Of the 40 patients, 13 were referred for tumor assessment, 6 for vascular related issues including arteriovenous malformations, stroke, vasculitis, and venous thrombosis, and 5 for hypoxic ischemic encephalopathy and premature birth. The remainder included referrals for headaches from unknown sources, sickle cell anemia, neurofibromatosis type 2, deafness and tinnitus, hemiparesis, esotropia, seizures, and preseptal cellulitis/dacryocystitis. Data from 37 cases were acquired on a 3 Tesla Siemens Prisma® scanner (software version VE11C, Siemens Medical Solutions, Erlangen, Germany), using a 64-channel head coil array. Three cases of data were acquired on a 3 Tesla Siemens Skyra® platform. Patients were in a standard supine position with head-first entry into the magnet bore. Imaging parameters for the multi-delay pCASL 3D Gradient and Spin Echo (GRASE) pulse sequence are summarized in Table 1, and are

Table 3
A summary of Pearson correlation coefficients (r^2) for regional ATT between linear weighted-delay mapping and non-linear iterative fitting computations. For each entry, slope (m) and intercept (b) are provided. Also provided in brackets are the 95% confidence intervals of the slope (m) and the intercept (b). Confidence intervals (CIs) that contain 1 for slope and 0 for intercept are italicized. All correlations were statistically significant with $p < 0.05$.

Perfusion territory	Left brain r^2/m/b [m: 95% CI], [b: 95% CI]	Right brain r^2/m/b [m: 95% CI], [b: 95% CI]
Anterior cerebral artery	0.92/1.01/0.09 [*m: 0.91, 1.11*], [b: 0.02, 0.16]	0.95/1.03/0.08 [*m: 0.95, 1.11*], [b: 0.02, 0.14]
Anterior choroidal artery	0.93/1.02/0.09 [*m: 0.93, 1.11*], [b: 0.02, 1.56]	0.93/1.05/0.07 [*m: 0.96, 1.14*], [*b: −0.01, 0.14*]
Posterior cerebral artery	0.90/1.01/0.07 [*m: 0.90, 1.11*], [*b: −0.02, 0.16*]	0.90/1.03/0.05 [*m: 0.92, 1.13*], [*b: −0.04, 0.14*]
Middle cerebral artery	0.99/0.91/2.27 [m: 0.87, 0.94], [b: 1.05, 3.48]	0.98/0.89/2.26 [m: 0.85, 0.94], [b: 0.74, 3.78]
Posterior communicating artery	0.95/1.03/0.07 [*m: 0.96, 1.11*], [b: 0.01, 0.13]	0.93/1.04/0.07 [*m: 0.94, 1.13*], [*b: −0.00, 0.14*]
Insula	0.93/1.04/0.10 [*m: 0.94, 1.13*], [*b: 0.04, 0.16*]	0.92/1.02/0.11 [m: 0.92, 1.12], [b: 0.05, 0.17]
Caudate nucleus	0.88/0.97/0.12 [*m: 0.85, 1.08*], [b: 0.03, 0.21]	0.91/1.03/0.09 [*m: 0.92, 1.13*], [b: 0.01, 0.17]
Lentiform nucleus	0.87/1.02/0.09 [*m: 0.90, 1.15*], [b: 0.00, 0.17]	0.90/1.04/0.08 [*m: 0.93, 1.15*], [b: 0.01, 0.15]
Internal capsule	0.89/1.04/0.06 [*m: 0.95, 1.16*], [*b: −0.02, 0.15*]	0.90/1.00/0.10 [*m: 0.90, 1.11*], [*b: 0.02, 0.18*]
M1	0.90/0.98/0.10 [*m: 0.88, 1.09*], [b: 0.02, 0.18]	0.93/1.02/0.07 [m: 0.93, 1.11], [b: 0.01, 0.14]
M2	0.93/1.02/0.08 [*m: 0.94, 1.11*], [b: 0.02, 0.14]	0.93/1.02/0.07 [*m: 0.94, 1.11*], [b: 0.01, 0.14]
M3	0.93/0.96/0.10 [*m: 0.87, 1.04*], [b: 0.03, 0.17]	0.90/0.98/0.08 [*m: 0.88, 1.08*], [*b: −0.01, 0.17*]
M4	0.96/1.08/0.02 [*m: 1.01, 1.15*], [*b: −0.04, 0.08*]	0.96/1.09/0.02 [*m: 1.02, 1.16*], [*b: −0.03, 0.08*]
M5	0.95/1.05/0.05 [*m: 0.98, 1.12*], [*b: −0.01, 0.12*]	0.96/1.07/0.03 [*m: 1.00, 1.14*], [*b: −0.03, 0.08*]
M6	0.96/0.97/0.10 [*m: 0.91, 1.03*], [b: 0.04, 1.55]	0.96/1.01/0.06 [*m: 0.94, 1.08*], [*b: −0.01, 0.12*]

similar to previous literature descriptions [23]. An image set (without RF labeling) was also acquired. The sequence was acquired prior to Gadolinium contrast administration.

Post-processing of the multi-phase 3D GRASE pCASL data was performed offline using a Java-based software package called CereFlow (Translational MRI, LLC, Los Angeles, CA). First, label and control paired ASL images were corrected for motion and physiological noise using principal component analysis [28]. Subsequently, pairwise subtraction between label and control images was performed, followed by averaging to generate the mean difference data set for each of the five PLDs. Two algorithms were then employed to quantitatively compute the CBF and the ATT. The first is a standard nonlinear iterative curve-fitting approach based on the classic single-compartment perfusion model [10,29–31]. The second approach is a linear method using a weighted-delay approach that leverages a monotonic function between the weighted-delay and the ATT [22,23,32]. Fig. 1 provides a simplified schematic of the two algorithms.

The computed CBF and ATT maps from both iterative and linear weighted-delay approaches were then normalized into a canonical space of the Montreal Neurological Institute template for children 3 years of age and above using the normalization function implemented in SimpleITK (http://www.simpleitk.org/). For subjects below 3 years of age, the CBF and ATT maps were normalized into the University of North Carolina “0-1-2 infant atlas” (https://www.nitrc.org/projects/pediatricatlas) based on their respective age. Once normalized, an additional template of cerebral vascular territories was applied to extract the average CBF and ATT values in the following regions: leptomeningeal and perforating anterior cerebral artery, leptomeningeal and perforating middle cerebral artery, posterior cerebral artery, anterior choroidal artery and posterior communicating artery on both hemispheres respectively [23]. Furthermore, the Alberta Stroke Program Early CT Score system was applied to extract average CBF and ATT values in M1-M6 perfusion territories, the caudate nucleus, the lentiform nucleus, and the internal capsule [33,34]. All post-processing steps were performed on a personal computer operating with a 3.6 GHz processor and 24 GB of memory.

The STATA statistical software package (Version 13, College Station, Texas) was used to perform linear regression and compare CBF and ATT measurements between the two estimation methods. A p-value of 0.05 was chosen to reflect statistical significance. Finally, a pediatric neuroradiologist with over 25 years of clinical experience retrospectively reviewed all ASL data along with conventional MRI data to determine in which cases the CBF and ATT information provided added diagnostic value.

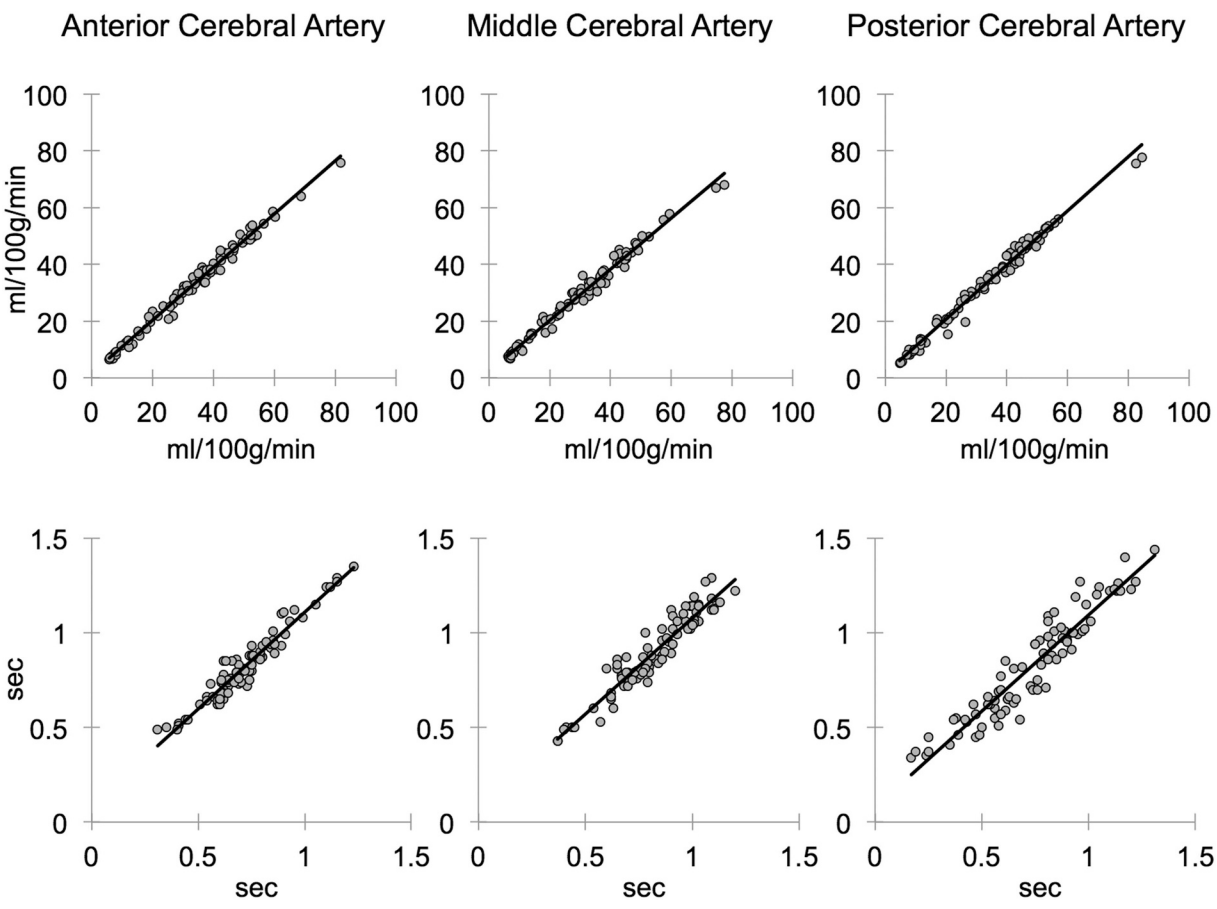

Fig. 2. Representative correlation plots of anterior cerebral artery, the middle cerebral artery, and the posterior cerebral artery perfusion regions for CBF (top) and ATT (bottom). Data from both left and right hemispheres are plotted together. Iterative fitting results plotted on x-axis, weighted-delay results plotted on y-axis.

3. Results

CBF and ATT maps were successfully reconstructed in all cases and were deemed of diagnostic quality based on review by a neuroradiologist. Average reconstruction time for the iterative curve-fitting approach was 3.2 min, in comparison to the weighted-delay method, which averaged 3.4 min, for each data set. Table 2 provides a summary of linear regression results between weighted-delay and curve-fitting estimates of CBF. Data is presented for the entire patient cohort, but separated based on left and right brain hemispheres as well as perfusion territories. ATT results are similarly presented in Table 3. In each table, the correlation coefficient, the regression line slope, and the regression line intercept, are presented. A perfect correlation between the estimates would yield a coefficient of 1, a slope of 1, and an intercept of 0. In brackets, the 95% confidence interval of the slope and the intercept are provided. Those entries that include 1.0 within the confidence interval for slope and 0 within the confidence interval for intercept are italicized. Overall, weighted-delay CBF measurements slightly underestimate those from iterative curve-fitting, with the greatest differences (poorest correlations) seen in the lentiform nucleus and the internal capsule. In contrast, weighted-delay ATT measurements in general slightly overestimated those from curve-fitting. Fig. 2 shows representative correlation plots of CBF and ATT for a few of the measured vascular territories, while accompanying Fig. 3 shows the corresponding Bland-Altman plots.

Figs. 4 through 7 subsequently illustrate representative examples from the patient cohort. Of the 40 cases, the neuroradiologist found CBF and ATT maps to be useful in providing additional diagnostic value in 17 patients. The quantitative ASL data highlighted asymmetric regional CBF and ATT patterns in cases involving stroke, sickle cell anemia, headaches, esotropia, photophobia, contusions, post-surgical venous infarct, premature birth, hypoxic ischemic encephalopathy, septic shocks, seizures, cerebral vasculitis, and hydrocephalus. In the remaining cases, the reviewing neuroradiologist noted normal appearing and symmetric CBF and ATT results, which did not provide additional diagnostic value beyond conventional morphological imaging.

4. Discussion

The primary goal of this work was to determine whether quantitative multi-phase 3D pCASL could be clinically utilized in children at our tertiary pediatric referral hospital. Our pilot study contributes knowledge to the literature, as multi-phase ASL has not been routinely applied in pediatric patients who possess significant CBF and ATT

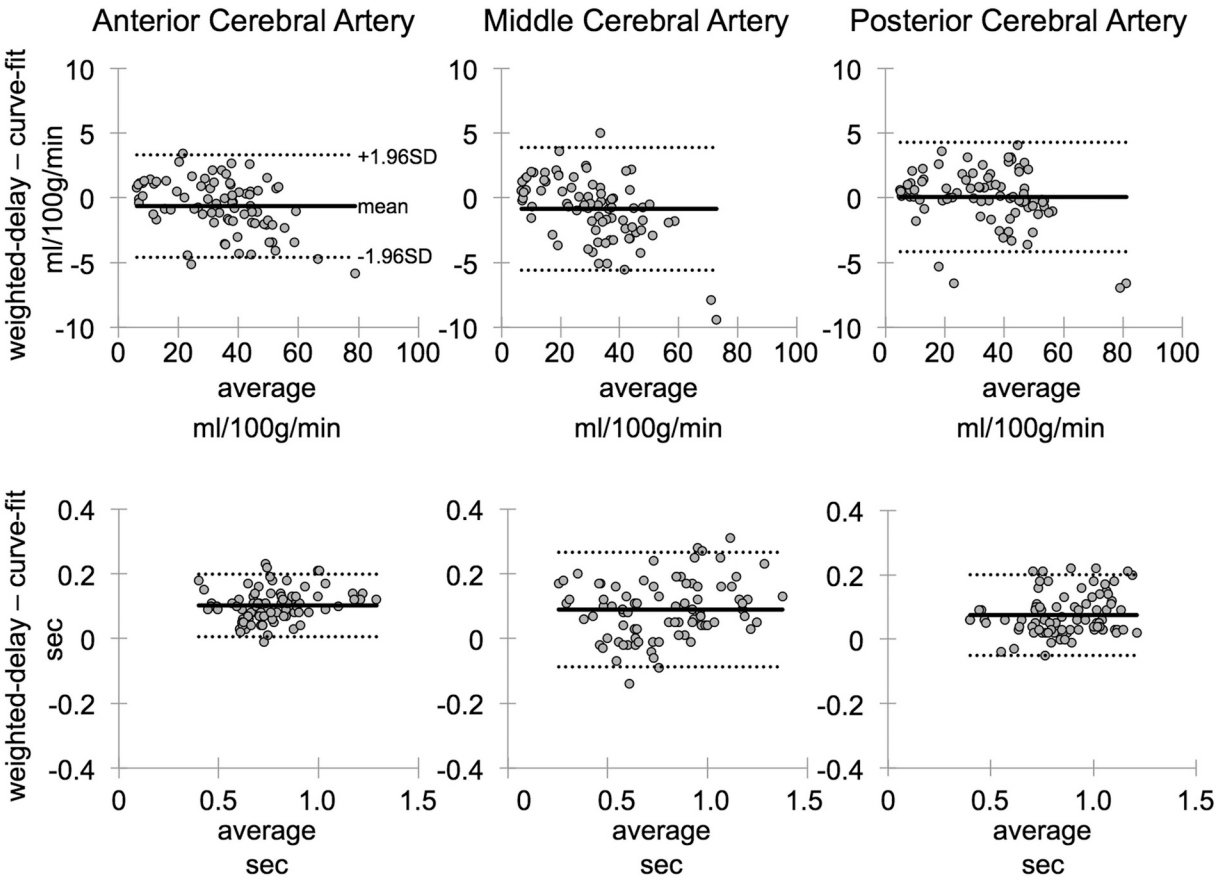

Fig. 3. Bland-Altman plots of CBF (top) and ATT (bottom) corresponding to the data presented in Fig. 2. Plots shown in a similar format.

variations. In this preliminary series of cases, data from all patients were successfully acquired, reconstructed, and presented to the reviewing neuroradiologist, and as a result, we are integrating multi-phase 3D ASL into our routine brain MRI protocols. The secondary purpose of this study was to compare estimations of CBF and ATT using a linear weighted-delay approach against a benchmark iterative non-linear curve-fitting technique. The former was originally proposed as an alternative means of estimating ATT when a limited number of delay times (< 5 PLDs) were used [22,23]. Our results herein suggest that both weighted-delay and curve-fitting methods can be reliably applied to pCASL data with 5 PLDs and yield comparable results in pediatric patients. Additionally, the computational and processing speed of both algorithms as implemented in the CereFlow software was comparable, at around 3–4 min per data set, and was deemed adequately quick for clinical workflow.

The optimal number of PLDs to employ in multi-phase ASL remains an active area of research as it needs to balance CBF and ATT accuracy, precision, and fidelity with scan time. In a recent study by van der Thiel, et al., the investigators showed systematic differences in CBF measurements between protocols using three versus seven PLDs [35]. In the literature, studies have reported using a broad range in the number of PLDs, from three in placental imaging [6], to four [22–25], six [18], seven [26], nine [27], and sixteen [16] in brain applications. Currently, there remains no consensus recommendation on the number of PLDs to use. It is likely dependent on anatomy and specific applications, as well as the underlying signal-to-noise ratio (SNR) of the underlying data and the magnitude of the anticipated CBF and ATT values. Studies towards standardization of application-specific multi-delay ASL protocols should be a direction of future work. Studies employing < 5 PLDs have used exclusively used the weighted-delay approach for CBF and ATT estimation, while those employing > 5 PLDs typically use iterative curve-fitting. In this work, we selected a protocol using five PLDs to achieve a reasonable scan time of 5–7 min. In the present work focusing on brain perfusion, we did not observe any major discrepancies or errors between the computed CBF and ATT maps from both weighted-delay or iterative curve-fitting algorithms. This is supported by the correlation plots in Fig. 2, the Bland-Altman plots in Fig. 3, and the linear regression statistics in Tables 2 and 3. The neuroradiologist on the study who reviewed all of the data was able to gain diagnostic information from either results.

We note several limitations in this study. First, we did not compare multi-phase ASL to dynamic susceptibility contrast MRI, the latter requiring an administration of Gadolinium contrast agent. Additional comparisons or sequences were not possible due to limited overall scan time, our patient volume, and clinical MRI schedule. Second, we did not involve a cohort of age- and gender-matched control subjects to compare CBF and ATT across groups. Having normative age- and gender-matched regional CBF and ATT values for comparison would have

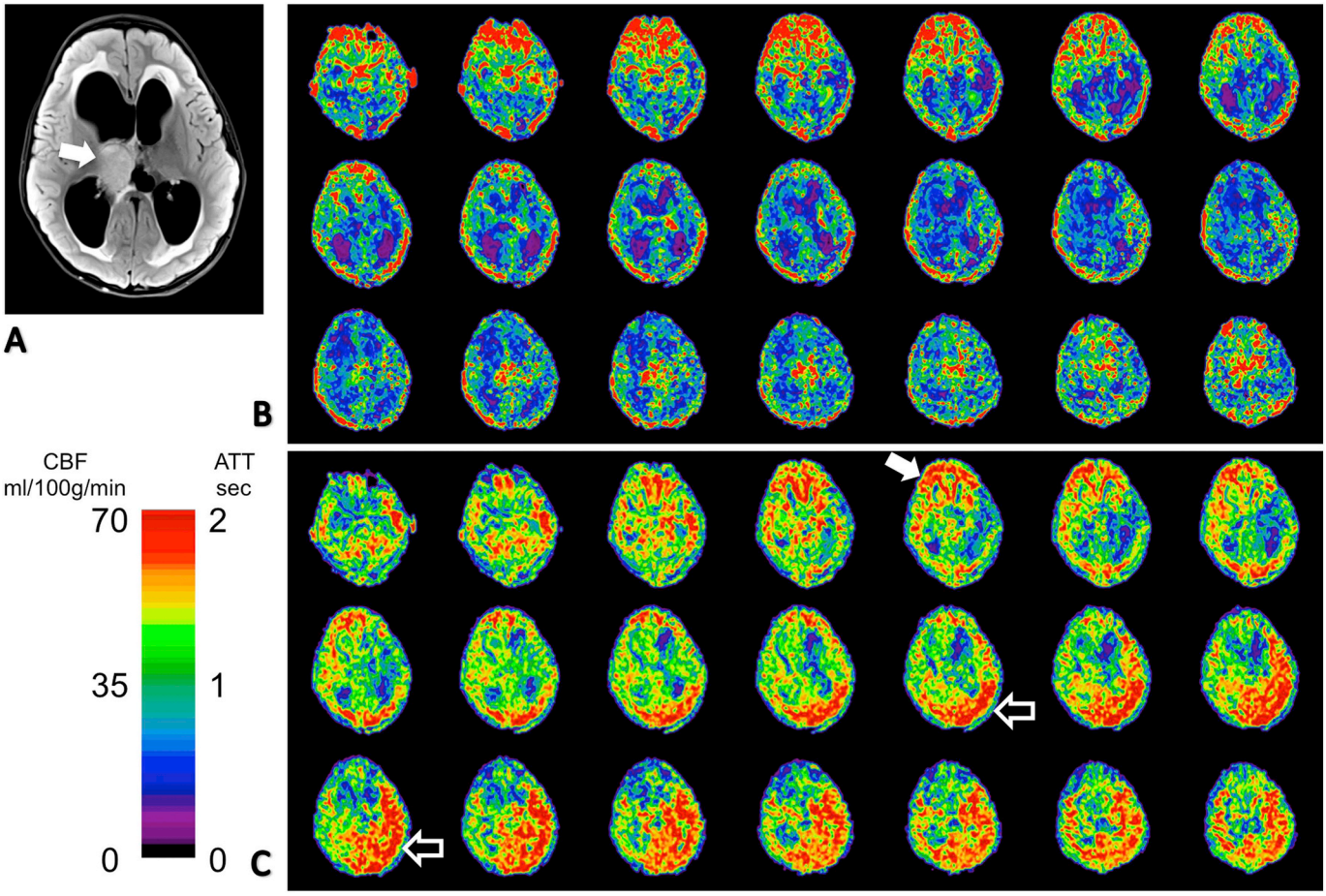

Fig. 4. Representative results from 7.5 years old female. (A) Patient is diagnosed with a mass lesion centered in the medial aspect of the right thalamus (arrow in A), as seen on FLAIR T2-weighted image. (B) CBF and (C) ATT from weighted-delay results. Note overall reduced CBF (global average is 31.8 ± 16.5 ml/100 g/min). CBF and ATT are shown using the same colorbar, but from 0 to 70 ml/100 g/min or 0–2 s, respectively. Note asymmetric ATT, with delayed transit notably on the left side (M4-M6 territories) (open arrow) and the right M1 and caudate regions (arrow in C) (For interpretation of the references to color in this figure legend, the reader is referred to the web version of this article.).

strengthened our work and provided clinical context into the various regional hypoperfusion, hyperperfusion observed in our patient cohort. Relatedly, we did not assess any patients longitudinally, and recognize that multi-phase ASL may be particularly useful in highlighting regional changes in CBF and ATT due to natural disease progression or therapeutic intervention. Third, although our sample size is arguably small, we do not feel that additional data will significantly alter the correlations we observed in CBF and ATT estimation between weighted-delay and curve-fitting routines. However, we acknowledge that additional studies are needed to expand and identify potential clinical applications of multi-phase ASL.

Fourth, arguably our current implementation of the imaging acquisition is relatively long at 5–7 min for whole-brain coverage. While most of our non-sedated patient cohort were able to cooperate and minimize head motion during this time period, shorter scan times can be had with additional data acceleration techniques, including single-shot pulse sequences with parallel imaging and compressed sensing [18,36], simultaneous multi-slice MRI [37] and MR fingerprinting [38,39]. Relatedly, we did not readily assess whether the linear weighted-delay or the nonlinear iterative least-squares curve-fitting algorithms for multi-phase 3D pCASL data was more robust in CBF and ATT estimation in regions of reduced SNR and in areas of extremely low CBF (i.e. white matter) and ATT. In the current work, we employed a signal averaging of two to three to achieve a scan time of 5–7 min with 5 PLDs. To achieve more SNR and improved robustness with either fitting algorithm, we believe that additional signal averaging in combination with a greater number of PLDs should be employed, at the expense of increased scan time or reduced slice coverage.

Lastly, we recognize that a portion of our patient cohort underwent their MRI exam under sedation and general anesthesia. The use of sedation and general anesthesia was solely determined based on patient condition by the attending anesthesiologist and the referring physician. The current study staff was not involved in any decision regarding sedation and anesthesia. While we recognize that sedation and anesthesia may impact a patient's brain perfusion characteristics [40], we do not believe such influence will affect the performance of multi-delay ASL as an imaging pulse sequence or the reconstruction algorithms that generate quantitative CBF and ATT maps. However, whether or not perfusion metrics were obtained in the absence or presence of sedation and general anesthesia should definitely be considered when comparing

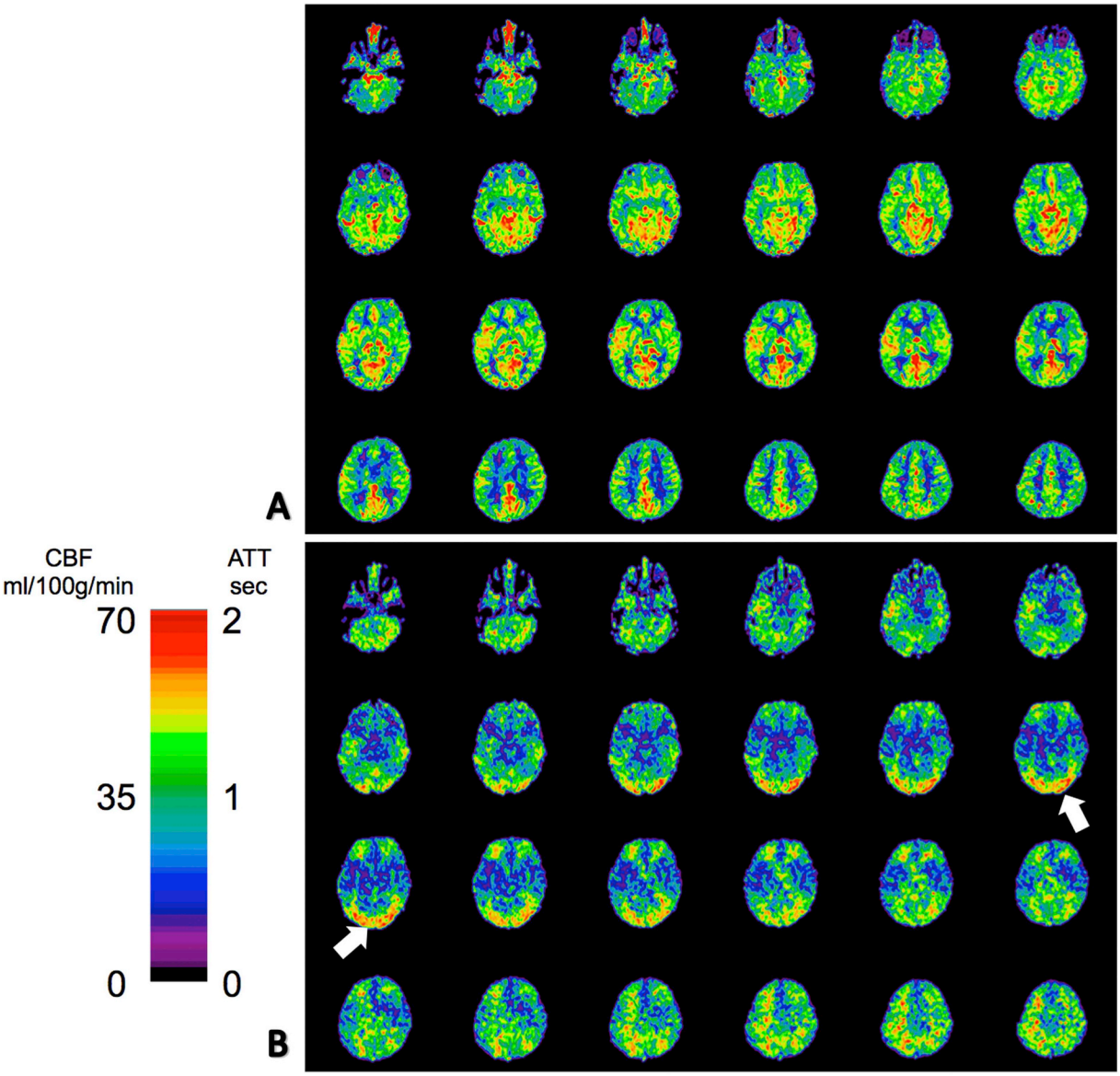

Fig. 5. Representative results from a 3 years old male, referred for assessment of afebrile seizures. MRI brain exam reported negative findings. Note global CBF in (A) is quite robust 37.1 ± 13.6 ml/100 g/min across the brain. ATT shows slightly increased transit times in the M3 territories and the leptomeningeal areas perfused by PCA (arrows).

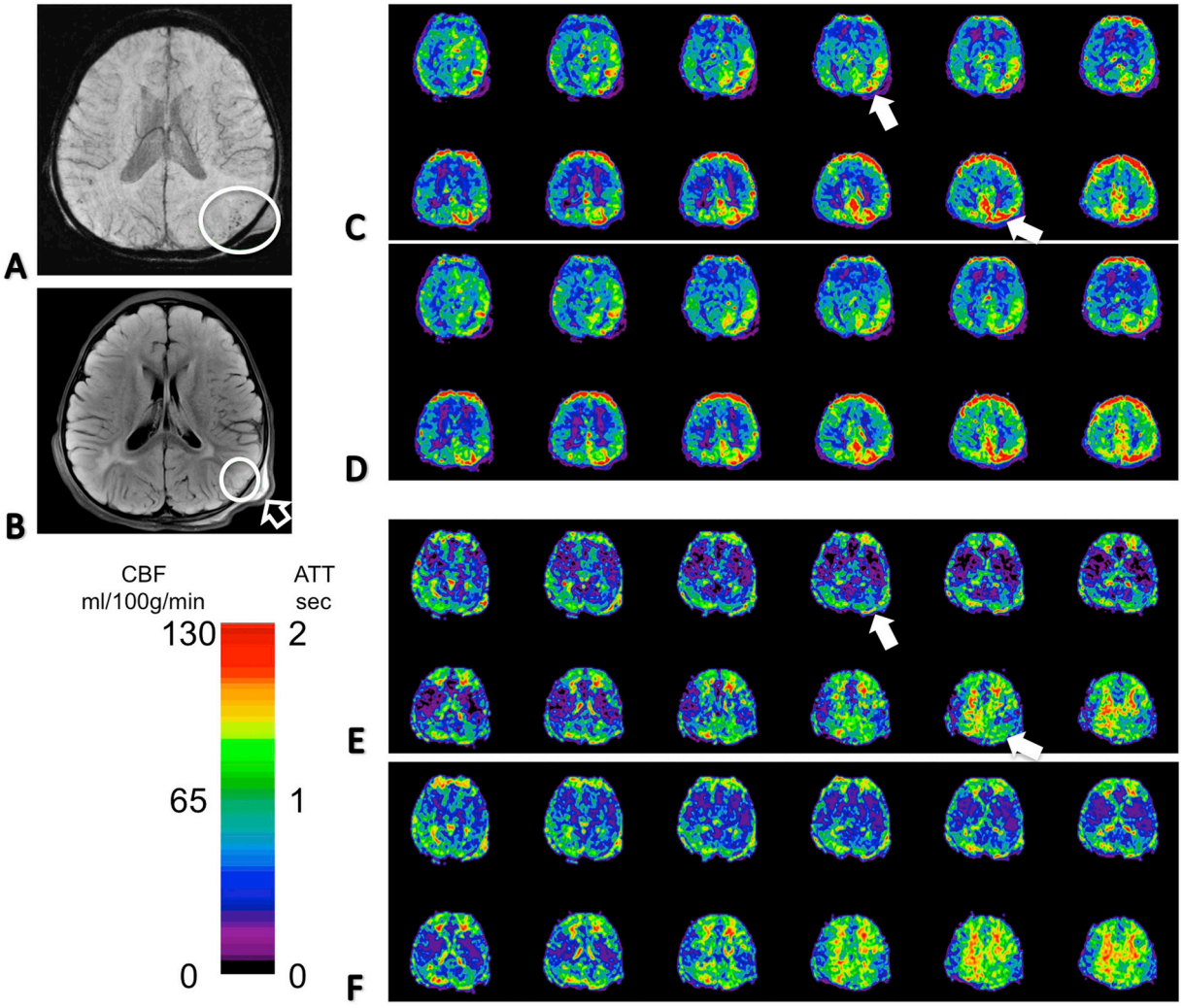

Fig. 6. Representative example from a 1.6 years old female referred to MRI for evaluation of brain trauma and cerebrovascular concerns. (A) Susceptibility weighted MRI demonstrates several punctate hemorrhagic foci within the contusion (circled region). (B) A region of hyperintensity (circled region) is seen on T2 FLAIR images in the left parietal cortex immediately beneath the patient's scalp edema. Comparative results of (C, D) CBF and (E, F) ATT maps derived from (C, E) iterative fitting and (D, F) weighted-delay methods. Abnormal increased perfusion within the left parietal cortex extending into the left occipital and temporal cortices (arrows) can be seen. Patient has normal vessel patency of all intracranial arteries with no concerns for stenosis, truncation, or dissection. Note the similarity of maps between iterative fitting and weighted-delay methods. ATT maps appear symmetric overall, but with a slight hint of asymmetry in the affected regions (i.e., increased CBF region appears to have slightly reduced ATT).

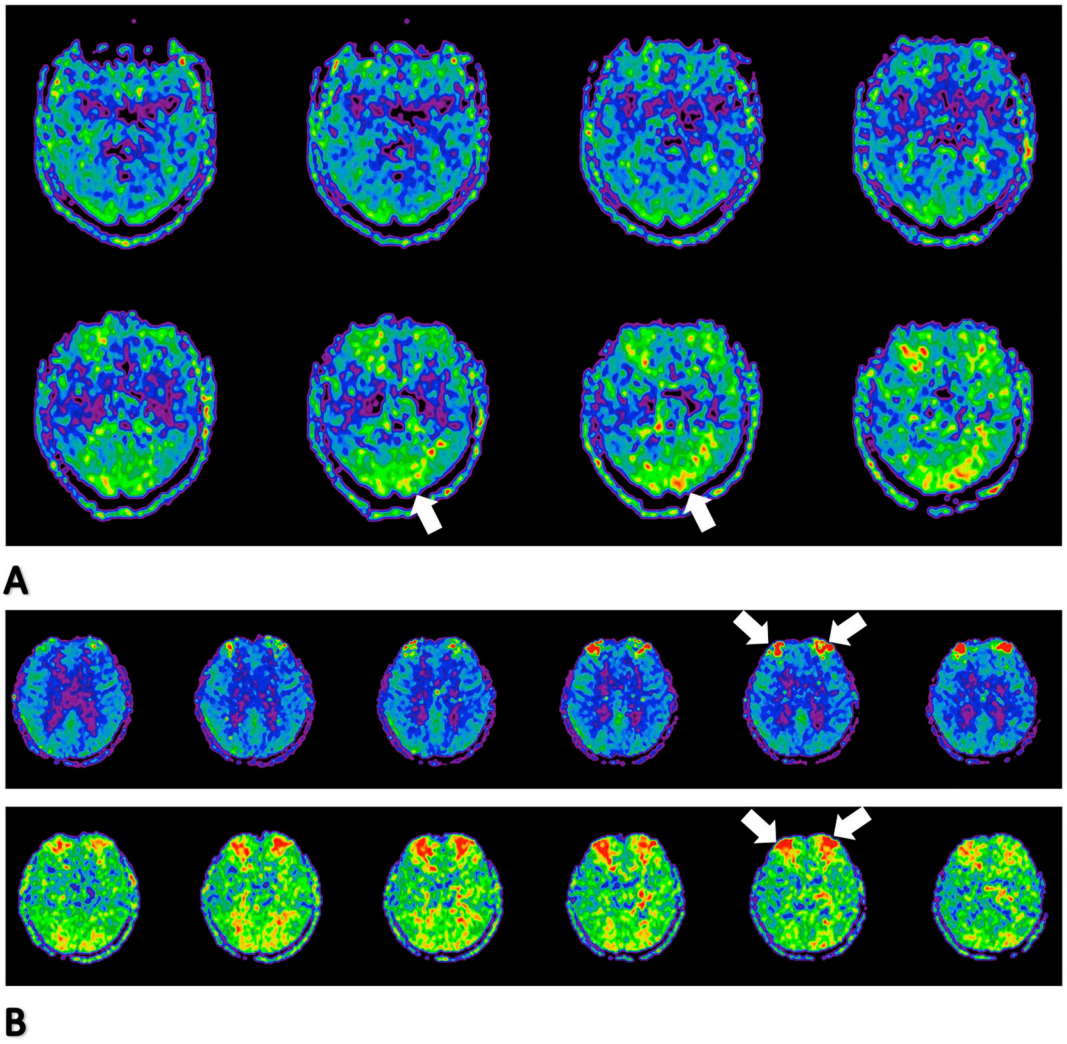

Fig. 7. Representative example from (A) a 6.5 years old female with complaints of severe headaches one day prior to MRI exam and history of photophobia. ATT maps show longer transit times in the watershed zones including the occipital areas (arrows). (B) 13.7 years old female with complaints of bifrontal lobe headaches. CBF and ATT maps show abnormal increase in both parameters in the frontal lobe (arrows). Same color scales for CBF and ATT as Fig. 5 (For interpretation of the references to color in this figure legend, the reader is referred to the web version of this article.).

measurements cohorts, both serially and longitudinally.

In conclusion, 3D multi-phase ASL has provided our neuroradiology practice with an additional tool that can be reliably applied in pediatric patients to estimate multi-parametric perfusion measurements in assessing neurological, vascular, and developmental disorders.

Conflict of interest declaration

The Department of Radiology at Nationwide Children's Hospital acknowledges research and funding support from Siemens Medical Solutions. Danny JJ Wang is a shareholder of Translational MRI LLC, which provided the software for post-processing of multi-delay pCASL data.

Acknowledgments

The authors would like to thank the Imaging Research Office of Nationwide Children's Hospital for research assistance. The authors are grateful to the MRI technologists, nurses, and staff of Nationwide Children's Hospital's Department of Radiology for their efforts and support.

References

[1] Ho ML. Arterial spin labeling: clinical applications. J Neuroradiol 2018. https://doi.org/10.1016/j.neurad.2018.06.003.
[2] Havsteen I, Nybing J, Christensen H, Christensen AF. Acta Radiol 2018. https://doi.org/10.1177/0284185117752552.
[3] Hernandez-Garcia L, Lahiri A, Schollenberger J. Recent progress in ASL. Neuroimage 2018. https://doi.org/10.1016/j.neuroimage.2017.12.095.
[4] Jezzard P, Chappell MA, Okell TW. Arterial spin labeling for the measurement of cerebral perfusion and angiography. J Cereb Blood Flow Metab 2018;38:603–26.
[5] Zun Z, Limperopoulos C. Placental perfusion imaging using velocity-selective arterial spin labeling. Magn Reson Med 2018;80:1036–47.
[6] Shao X, Liu D, Martin T, et al. Measuring human placental blood flow with multi-delay 3D GRASE pseudocontinuous arterial spin labeling at 3T. J Magn Reson Imaging 2018;47:1667–76.
[7] Campbell-Washburn AE, Zhang H, Siow BM, et al. Multislice cardiac arterial spin labeling using improved myocardial perfusion quantification with simultaneously measured blood pool input function. Magn Reson Med 2013;70:1125–36.
[8] Kober F, Jao T, Tralen T, Nayak KS. Myocardial arterial spin labeling. J Cardiovasc Magn Reson 2016. https://doi.org/10.1186/s12968-016-0235-4.
[9] Nery F, Gordon I, Thomas DL. Non-invasive renal perfusion imaging using arterial spin labeling MRI: challenges and opportunities. Diagnostics (Basel) 2018. https://doi.org/10.3390/diagnostics8010002.
[10] Alsop DC, Detre JA, Golay X, et al. Recommended implementation of arterial spin-labeled perfusion MRI for clinical applications: a consensus of the ISMRM perfusion study group and the European consortium for ASL in dementia. Magn Reson Med 2015;73:102–16.

[11] Lee S, Yun TJ, Yoo RE, et al. Monitoring cerebral perfusion changes after revascularization patients with Moyamoya disease by using arterial spin-labeling MR imaging. Radiology;228:565–572.
[12] Juttukonda MR, Jordan LC, Gindville MC, et al. Cerebral hemodynamics and pseudo-continuous arterial spin labeling considerations in adults with sickle cell anemia. NMR Biomed 2017;30. https://doi.org/10.1002/nbm.3681.
[13] Taki Y, Hashizume H, Sassa Y, et al. Correlation between gray matter density-adjusted brain perfusion and age using brain MR images of 202 healthy children. Hum Brain Mapp 2011;32:1973–85.
[14] Carsin-Vu A, Corouge I, Commowick O, et al. Measurement of pediatric regional cerebral blood flow from 6 months to 15 years of age in a clinical population. Eur J Radiol 2018;101:38–44.
[15] Liu F, Duan Y, Peterson BS, et al. Resting state cerebral blood flow with arterial spin labeling MRI in developing human brains. Eur J Paediatr Neurol 2018;22:642–51.
[16] Shen Y, Zhao B, Yan L, et al. Cerebral hemodynamic and white matter changes of Type 2 diabetes revealed by multi-TI arterial spin labeling and double inversion recovery sequence. Front Neurol 2017. https://doi.org/10.3389/fneur.2017.00717.
[17] Yun TJ, Sohn CH, Yoo RE, et al. Transit time corrected arterial spin labeling technique aids to overcome delayed transit time effects. Neuroradiology 2018;60:255–65.
[18] Boland M, Stirnberg R, Pracht ED, et al. Accelerated 3D-GRASE imaging improves quantitative multiple post labeling delay arterial spin labeling. Magn Reson Med 2018. https://doi.org/10.1002/mrm.27226.
[19] Wolfe ME, Layer V, Gregori J, et al. Assessment of perfusion deficits in ischemic stroke using 3D-GRASE arterial spin labeling magnetic resonance imaging with multiple inflow times. J Neuroimaging 2014;24:453–9.
[20] Martin Z, Madai VI, Samson-Himmelstjerna FC, et al. 3D GRASE pulsed arterial spin labeling at multiple inflow times in patients with long arterial transit times: comparison with dynamic susceptibility-weighted contrast-enhanced MRI at 3 Tesla. J Cereb Blood Flow Metab 2015;35:392–401.
[21] Federau C, Christensen S, Zun Z, et al. Cerebral blood flow, transit time, and apparent diffusion coefficient in Moyamoya disease before and after acetazolamide. Neuroradiology 2017;59:5–12.
[22] Wang R, Yu S, Alger JR, et al. Multi-delay arterial spin labeling perfusion MRI in Moyamoya disease – comparison with CT perfusion imaging. Eur Radiol 2014;24:1135–44.
[23] Wang DJ, Alger JR, Qiao JX, et al. Multi-delay multi-parametric arterial spin-labeled perfusion MRI in acute ischemic stroke – comparison with dynamic susceptibility contrast enhanced perfusion imaging. Neuroimaging Clin N Am 2013;3:1–7.
[24] Lou X, Yu S, Scalzo F, et al. Multi-delay ASL can identify leptomeningeal collateral perfusion in endovascular therapy of ischemic stroke. Oncotarget 2017;8:2437–43.
[25] Chen G, Lei D, Ren J, et al. Patterns of postictal cerebral perfusion in idiopathic generalized epilepsy: a multi-delay multi-parametric arterial spin labelling perfusion MRI study. Sci Rep 2016. https://doi.org/10.1038/srep28867.
[26] Choi HJ, Sohn CH, You SH, et al. Can arterial spin-labeling with multiple post-labeling delays predict cerebrovascular reserve? AJNR Am J Neuroradiol 2017. https://doi.org/10.3174/ajnr.A5439.
[27] MacIntosh BJ, Pattinson KT, Gallichan D, et al. Measuring the effects of remifentanil on cerebral blood flow and arterial arrival time using 3D GRASE MRI with pulsed arterial spin labelling. J Cereb Blood Flow Metab 2008;28:1514–22.
[28] Shao X, Tisdall MD, Wang DJ, van der Kouwe AJW. Prospective motion correction for 3D GRASE pCASL with volumetric navigators. Proc Int Soc Magn Reson Med Sci Meet Exhib 2017;25:0680.
[29] Buxton RB, Frank LR, Wong EC, Siewert B, Warach S, Edelman RR. A general kinetic model for quantitative perfusion imaging with arterial spin labeling. Magn Reson Med 1998;40:383–96.
[30] Ji J, Pham V, Zhu XP, Li KI. Parameter estimation in arterial spin labeling MRI: comparing the four phase model and the Buxton model with Fourier transform. Quant Imaging Med Surg 2011;1:17–23.
[31] Buxton RB. Quantifying CBF with arterial spin labeling. J Magn Reson Imaging 2005;22:723–6.
[32] Dai W, Robson PM, Shankaranarayanan A, Alsop DC. Reduced resolution transit delay prescan for quantitative continuous arterial spin labeling perfusion imaging. Magn Reson Med 2012;67:1252–65.
[33] Aviv RI, Mandelcorn J, Chakraborty S, et al. Alberta stroke program early CT scoring of CT perfusion in early stroke visualization and assessment. AJNR Am J Neuroradiol 2007;28:1975–80.
[34] Yu S, Ma SJ, Liebeskind DS, et al. ASPECTS-based reperfusion status on arterial spin labeling is associated with clinical outcome in acute ischemic stroke patients. J Cereb Blood Flow Metab 2018;38:382–92.
[35] Van der Thiel M, Rodriguez C, Giannakopoulos P, et al. Brain perfusion measurements using multidelay arterial spin-labeling are systematically biased by the number of delays. AJNR Am J Neuroradiol 2018;39:1432–8.
[36] Shao X, Wang DJ. Single shot high resolution 3D arterial spin labeling using 2D CAIPI and ESPIRiT reconstruction. Proc Int Soc Magn Reson Med 2017;25:3629.
[37] Feinberg DA, Beckett A, Chen L. Arterial spin labeling with simultaneous multi-slice echo planar imaging. Magn Reson Med 70;1500–1506.
[38] Su P, Mao D, Liu P, Li Y, Pinho MC, Welch BG, et al. Multiparametric estimation of bray hemodynamics with MR fingerprinting ASL. Magn Reson Med 2017;78:1812–23.
[39] Wright KL, Jiang Y, Ma D, Noll DC, Griswold MA, Gulani V, et al. Estimation of perfusion properties with MR fingerprinting arterial spin labeling. Magn Reson Med 2018;50:68–77.
[40] Harreld JH, Helton KJ, Kaddoum RN, et al. The effects of propofol on cerebral perfusion MRI in children. Neuroradiology 2013;55:1049–56.